Bioorganic & Medicinal Chemistry 18 (2010) 7716–7723

Contents lists available at ScienceDirect

Bioorganic & Medicinal Chemistry

journal homepage: www.elsevier.com/locate/bmc

Structural and functional characterization of a synthetically modified OmpG

Wolfgang Grosse, Philipp Reiß, Simon Reitz, Menekse Çebi, Wolger Lübben, Ulrich Koert *, Lars-Oliver Essen *

Philipps-Universität Marburg, Fachbereich Chemie, Hans-Meerwein-Straße, 35032 Marburg, Germany

ARTICLE INFO

Article history:
Received 19 October 2009
Revised 15 March 2010
Accepted 17 March 2010
Available online 25 March 2010

Keywords:
Ion-channel engineering
OmpG hybrids
Crystal structure
Membrane protein

ABSTRACT

Chemical modification of ion channels has recently attracted attention due to their potential use in stochastic sensing and neurobiology. Among the available channel templates stable β-barrel proteins have shown their potential for large scale chemical modifications due to their wide pore lumen. Ion-channel hybrids using the outer membrane protein OmpG were generated by S-alkylation with a synthetic modulator and functionally as well as structurally characterized. The dansyl moiety of the used modulator resulted in partial blockage of current though the OmpG channel with its gating characteristics mainly unaffected. The crystal structure of an OmpG–**dansyl** hybrid at 2.4 Å resolution correlates this finding by showing that the modulator lines the inner walling of the OmpG pore. These results underline the suitability of OmpG as a structural base for the construction of stochastic sensors.

1. Introduction

During the last years the chemical modification of ion channels has gained great interest due to their promising use in sensing and neurobiology.[1] Often, this form of ion-channel engineering was limited to channels with narrow diameters.[2] Alternatively, porins from outer membranes of gram-negative bacteria with their robust β-barrel structure and their wider transmembrane channels have proven their potential in the use as stochastic sensors. These channels provide diverse architectures and diameters thus allowing the tailoring towards different applications.[1,3–5] So far, the best described system is α-hemolysin (αHL), a heptameric pore.[1,6–9] On the level of single molecules, this system, where the 14-stranded transmembrane channel is built up of seven αHL subunits, allowed, for example, stochastic sensing, light-triggered switching or tracking of single molecule reactions. Recently, similar studies on OmpF incorporating synthetic modulators have been reported.[10] OmpF forms highly stable trimers with each pore being composed of a single subunit. OmpG from *Escherichia coli* resembles in its architecture OmpF, but due to its monomeric nature it is an appealing target for single-molecule detection as it lacks the putative disadvantages of the oligomeric systems described above.[11–15]

The outer membrane protein OmpG comprises of 280 amino acids forming a stable β-barrel structure with 14 antiparallel β-sheets. The monomeric OmpG pore shows short turns and N- and C-termini on the inner, periplasmic side, but longer loops on the outer, extracellular side. Due to its large pore with a diameter of ~11 × 15 Å this porin is rather unspecific by allowing the transport of nutrients, especially sugars, up to a mass of 600 Da. Unlike trimeric OmpF, the transmembrane channel of OmpG lacks a constriction zone narrowing the central region of the pore and provides a simpler, cylindrical architecture instead of the hour-glass cross section of OmpF. In single-channel recordings OmpG shows a comparable conductivity of 0.8 nS in 1 M NaCl and, as a hallmark of the electrophysiological characteristics of OmpG, a strong gating behavior, that is, flickering, caused by the L6 loop.[11,13–17]

Overall, the outstanding difference to other β-barrel porins like α-HL and OmpF is the monomeric quaternary structure of OmpG, because this facilitates the simple and non-symmetric modification of distinct positions in the pore via mutagenesis and chemical modification. Unlike oligomeric porins, homogenic behavior in single-channel recordings due to incomplete modification can be hence ruled out.

So far, OmpG is the only monomeric porin used for ion-channel engineering.[18,19] Bayley and co-workers demonstrated cyclodextrin-dependent ADP detection and examined membrane insertion.[20] The latter authors also showed a way to overcome the intrinsic problem of OmpG, its flickering, by stabilizing its L6 loop

Abbreviations: αHL, α-hemolysin; BLM, black lipid membrane; C_8E_4, *n*-octyltetraoxyethylene; Da, Dalton; DTT, dithiothreitole; EDTA, ethylenediaminetetraacetic acid; HEPES, 2-(4-(2-hydroxyethyl)-1-pierazinyl)-ethanesulfonate; IPTG, isopropyl-β-D-thiogalactopyranoside; LDAO, lauryldimethylamine-oxide; *n*-OG, *n*-octyl-β-D-glucopyranoside; OmpF, outer membrane protein F; OmpG, outer membrane protein G; PEG, polyethyleneglycol; PMSF, phenylmethylsulfonylfluoride; SDS–PAGE, sodium dodecyl sulfate–polyacrylamide gel electrophoresis; TCEP, tris(2-carboxyethyl)phosphine; Tris, tris(hydroxymethyl)-aminomethane.

* Corresponding authors.
E-mail addresses: koert@chemie.uni-marburg.de (U. Koert), essen@chemie.uni-marburg.de (L.-O. Essen).

0968-0896/$ - see front matter © 2010 Elsevier Ltd. All rights reserved.
doi:10.1016/j.bmc.2010.03.044

by engineering a disulfide bond.[17] Here, we show the first covalently attached modification of OmpG with its structural as well as functional characterization.

2. Results and discussion

2.1. Construction of OmpG hybrids

Among the available pathways for engineering porin hybrids[10] the covalent modification of cysteines introduced by mutagenesis has turned out to be best suited for OmpG hybrids. The quantitative reaction of iodoacetamide-activated modulators with cysteines has been applied before to OmpF using a crown ether compound or the fluorescent compound dansyl (Fig. 1).[5,10] The other pathway of creating OmpF hybrids, native chemical ligation, resulted for OmpG only in low yields of hybrids so far (~10% after ligation, modification, refolding and purification, data not shown).

Using cysteine alkylation, the generation of OmpG–**dansyl** hybrids is possible in the folded state as well as under denaturing conditions (Fig. 2). However, modification of OmpG in 6 M urea has proven to be most efficient. Especially, the availability of large amounts of unfolded OmpG when overproduced as inclusion bodies, typical yields here are 60–90 mg/L^{-1} culture, makes this pathway extraordinarily interesting considering yields of up to 90% after refolding. Figure 1 shows the general procedure of OmpG modification as outlined in Section 4.

As attachment points for synthetic modulators two positions were assigned in the OmpG pore, M13 and Y209. These residues from β-strands 1 and 11 are centrally located in the β-barrel and were mutated to cysteines. The inward-facing of the side chains of these residues into the OmpG channel implies at least partial blockage, if voluminous modifications are synthetically introduced (Fig. 1).

The nearly quantitative formation of OmpG hybrids with the **dansyl** compound could be routinely performed with both mutants resulting in large amounts (~2 mg) as needed for functional and structural characterization. Figure 2 shows an SDS–PAGE gel of the obtained OmpG hybrids with the intrinsic fluorescence of the **dansyl** modification. Like the **OmpG** wild type, its **dansyl** hybrids demonstrated faster migration in SDS–PAGEs in the folded than in the unfolded state. A preference for one of the mutants could not be seen during refolding, purifying and characterizing OmpG hybrids, indicating that both introduced modifications do not interfere with the folding characteristics of OmpG.

Fluorescence spectra recorded for the OmpG–dansyl hybrids clearly demonstrated the quantitative incorporation of the fluorogenic **dansyl** group within the ion channel (Fig. 3). The emission maxima of the **OmpG/C209-dansyl** as well as of the **OmpG/C13-dansyl** hybrid differed by less than 3 nm from the emission maximum of the free dansyl compound (λ_{max} = 530 nm) and had no significant effect on the relative fluorescence yield. As the polarity of the surrounding medium is known to affect the fluorescence of the dansyl group, for example, in dansyl-hapten/antibody complexes relative shifts of up to 60 nm were observed,[21,22] one may infer that the dansyl groups are freely exposed into the aqueous pore lumen.

2.2. Functional characterization of OmpG hybrids

The conductance of OmpG hybrids was analyzed by single-channel recordings using the black lipid membrane (BLM) method. To establish the setup and check that OmpG refolding had no significant influence, for example, due to the presence of endogenous lipids, membrane-extracted wild type **OmpG** (data not shown) was compared to in vitro refolded **OmpG**. Both types of OmpG preparations showed comparable conductivities with a conductivity of

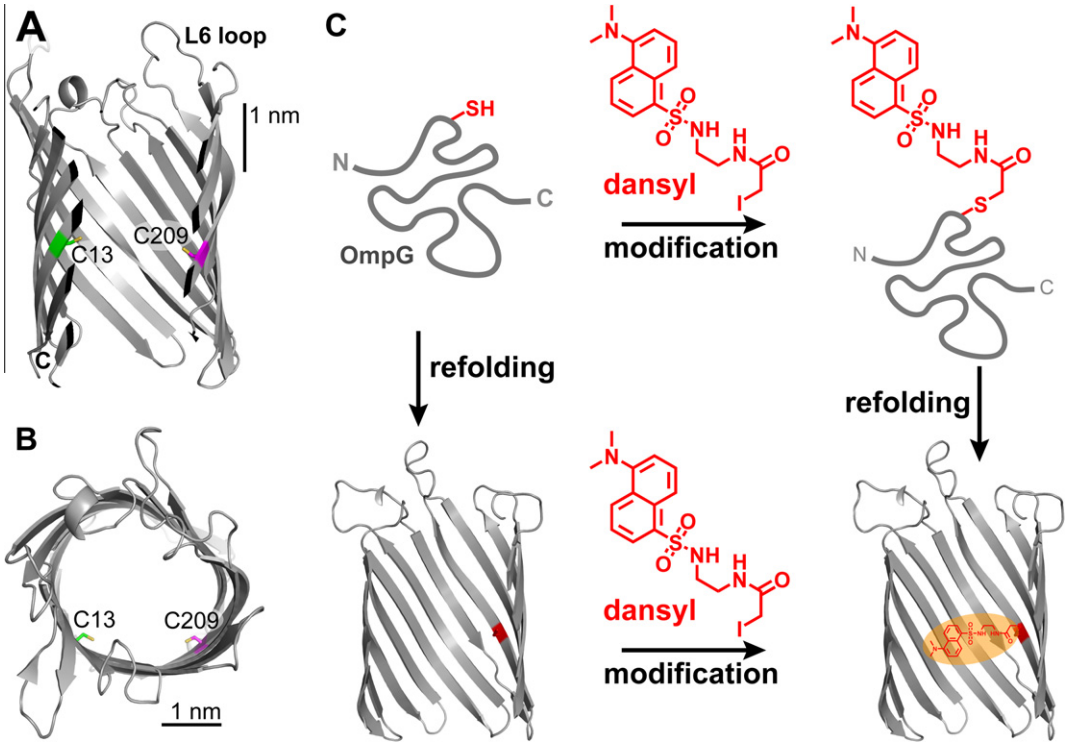

Figure 1. OmpG pore in the open state and pathways for chemical modification. (A) β-barrel from the side and (B) from the top. Single cysteine mutations are highlighted in green (C13) and pink (C209). The distance of modifications to the rim of the pore is ~15 Å. (C) Engineering of OmpG hybrids via alkylation of cysteine mutants by modification in denatured state (top) and in refolded state (bottom). The OmpG structure depicted here corresponds to the open state. Molecular graphics were created by PyMol (*Delano Scientific*) and based on the OmpG structure (pdb code 2IWV).[14]

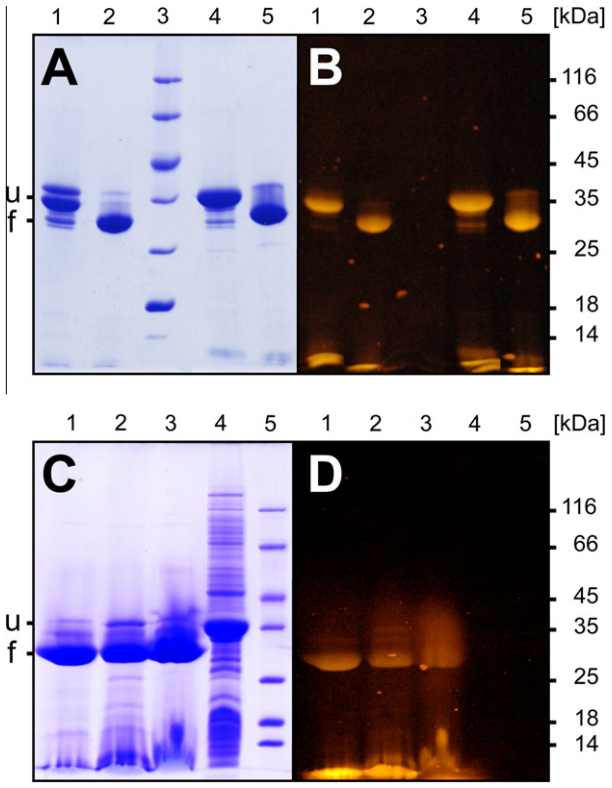

Figure 2. Denaturing 12% SDS–PAGE of the OmpG hybrids with the **dansyl** modification. (A) Coomassie-stained gel, (B) same gel examined under UV light (λ_{max} = 325 nm). The coupling reaction was performed in the denatured state. Lane 1: heat-denatured (u: unfolded) and lane 2: native sample (f: folded) of **OmpG/C13-dansyl**; lane 3: molecular weight marker; lane 4: heat-denatured and lane 5: native sample of **OmpG/C209-dansyl**. (C) Coomassie-stained gel, (D) same gel examined under UV light. Here, coupling was performed in the folded state. Lane 1: **OmpG/C13-dansyl**, lane 2: **OmpG/C209-dansyl**; lane 3: **OmpG + dansyl** showing no specific binding of the synthetic modulator; lane 4: heat-denatured **OmpG** and lane 5: molecular weight marker.

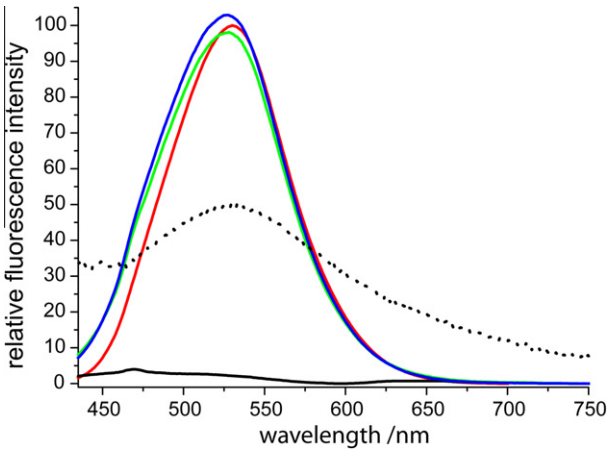

Figure 3. Fluorescence emission spectra of a **dansyl** reference (red, 200 μM) normalized to 100 and native **OmpG** (black, 90 μM), **OmpG/C13-dansyl** (green, 60 μM) and **OmpG_C209-dansyl** (blue, 90 μM) scaled to equal concentration as the dansyl reference. The emission peaks shift slightly from 530 nm for **dansyl** to 528 nm and 527 nm for **OmpG/C13-dansyl** and **OmpG/C209-dansyl**, respectively. The dashed line represents the fluorescence recorded at a single **OmpG/C209-dansyl** crystal at 18 °C. The latter was scaled to 50 with an apparent emission maximum at 533 nm. All spectra were measured by excitation at 405 nm wavelength.

0.74 ± 0.01 nS in 1 M NaCl for refolded **OmpG** serving as reference. This is consistent with values being reported before ranging from 0.81 nS by Conlan et al.[11,12] to 0.7 nS by Liang et al.[15] Slight differences might be caused by different lipids used for the BLM-measurements, different OmpG purification schemes or the setup in general.

The refolded cysteine mutants **OmpG/C13** and **OmpG/C209** were examined in the unmodified state by BLM measurements to check for intrinsic changes and verify their comparability to wild type **OmpG**. Interestingly, the measured conductivity of both cysteine mutants was slightly increased compared to refolded OmpG wild type. For **OmpG/C13** a value of 0.77 ± 0.1 nS and for **OmpG/C209** an even higher value of 0.82 ± 0.02 nS was determined as shown in Figure 4A. Considering the steric hindrance of the exchanged amino acids and their location in the middle of the OmpG β-barrel, the increase of conductivity fits well with their decrease in size.

Single-channel recordings of the OmpG hybrids showed reduced currents as compared to the unmodified cysteine mutants and OmpG wild type. Although a conductivity reduction was expected for a compound dwelling in the centre of the β-barrel and thus partly blocking the ion flow, the relatively small size of **dansyl** allowed no complete blockage. Nevertheless, there was a pronounced site-dependence for the introduction of synthetic modulators into the pore, indicating that the observed blockage efficiencies are not simply caused by volume changes within the pore. We determined a conductivity of 0.63 ± 0.03 nS for **OmpG/**

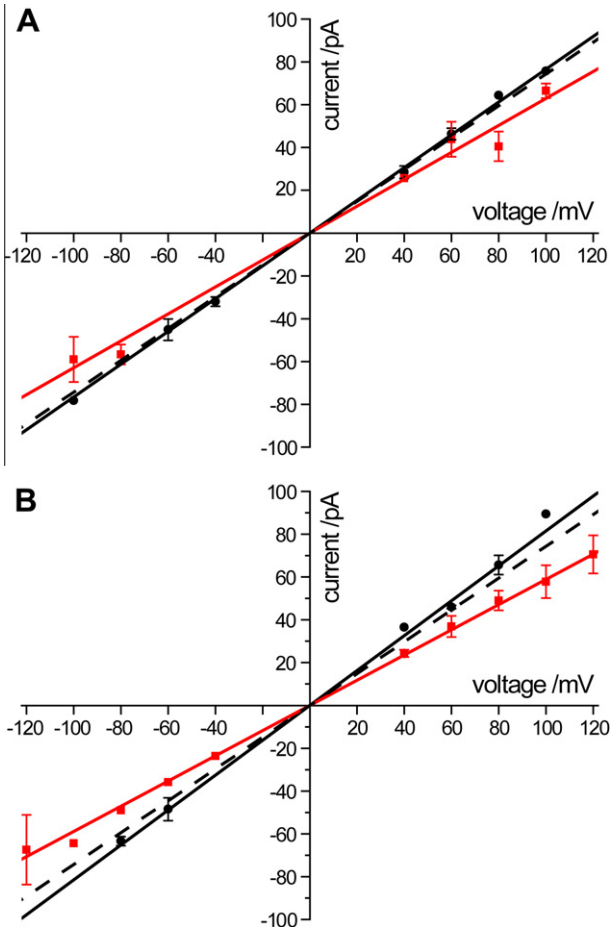

Figure 4. BLM measurements of OmpG hybrids. (A) **OmpG/C13** (black data points and line), **OmpG/C13-dansyl** (red squares and line) and **OmpG** (dashed line); conductivities: 0.77 ± 0.1 nS, 0.63 ± 0.03 nS and 0.74 ± 0.01 nS, respectively. (B) **OmpG/C209** (black data points and line), **OmpG/C209-dansyl** (red squares and line) and **OmpG** (dashed line); conductivities: 0.82 ± 0.02 nS, 0.59 ± 0.02 nS and 0.74 ± 0.01 nS.

C13-dansyl. This conductance corresponded to a reduction by 18% as compared to **OmpG/C13** (0.77 ± 0.1 nS) (Fig. 4A). In contrast, the **OmpG/C209** mutant showed larger effects reducing the current from 0.82 ± 0.02 nS in unmodified **OmpG/C209** by 28% to 0.59 ± 0.02 nS in **OmpG/C209-dansyl** (Fig. 4B). The significance of these deviations was validated via *t*-tests.

Apart from the observed overall conductance amplitudes, the dynamic behavior, particularly the flickering-characteristics, of the OmpG hybrids is similar to the wild type protein and unmodified mutants. The **dansyl** modification does not exhibit significant influence on the channel aside from reducing the overall conductivity as shown in Figure 5. Since the L6 loop is the dominant factor for fast gating[17] and the middle of the barrel is almost unaffected by the conformation of the L6 loop, as shown in OmpG structures of the closed and the open states of OmpG,[14] an effect on channel gating would have been surprising. Accordingly, the 2D-distribution plots for dwell times versus relative current amplitudes (Fig. 5) of **OmpG/C209** and **OmpG/C209-dansyl**, respectively, underlined that the dynamics of the OmpG hybrids remained mainly unaffected.

2.3. Structural analysis of OmpG/C209-dansyl

Crystallization of OmpG hybrids succeeded in sitting drop setups using the conditions for histidine-tagged OmpG from Subbarao et al.[13] This crystal form was chosen due to the option of OmpG-hybrid purification via affinity chromatography using the C-terminal His_6-tag. Both, **OmpG/C13-dansyl** and **OmpG/C209-dansyl**, yielded crystals in various conditions like membrane-extracted and refolded **OmpG**. OmpG hybrid crystals grew within about two weeks to thin plates, which tend to break easily like crystals of the OmpG wild type. Despite a satisfying crystallization tendency only few of these crystals showed proper diffraction with many crystals diffracting weakly or not at all. Only the **OmpG/C209** mutant attached to the **dansyl** modulator yielded well diffracting crystals sufficient for structural analysis. Single crystals of this hybrid were examined at the microspectrometer and showed the characteristic fluorescence of the **dansyl** modulator with an apparent λ_{max} of 533 nm (Fig. 3). The slight difference to the fluorescence observed in solution by about 6 nm might be caused by the slightly acidic pH and buffer composition as dictated by the crystallization condition.

The best diffracting crystal of **OmpG/C209-dansyl** grew in 50 mM cacodylate, pH 5.75, 1.2 M sodium formate and 28% PEG400. The space group (C2) and cell parameters of the obtained 2.4 Å dataset were almost identical as described before.[13] Accordingly, the therefrom calculated electron density showed a well defined β-barrel, where residues N4 to H283 were defined by electron density showing gaps in the L1, L2 and L6 loops due to intrinsic mobility. Compared to the search model (pdb code 2F1C) the L6 loop could be extended by 5 residues and the L7 loop was built anew. Despite missing residues in the L6 loop (W222-R228), its main chain conformation indicates an open state of the pore, where no intrusion into the pore can be expected for this loop under given conditions. Additionally, partly or completely defined density was found for seven detergent moieties and modeled along the crystal contacts formed by the OmpG molecules (Fig. 6). Apart from the **dansyl** modulator four alternative side chain conformations were found in OmpG and refined.

In position 209 additional difference density for the modulator was found as shown in Figure 6. The SIGMAA-weighted OMIT difference electron densities clearly show the linker-arm used for the

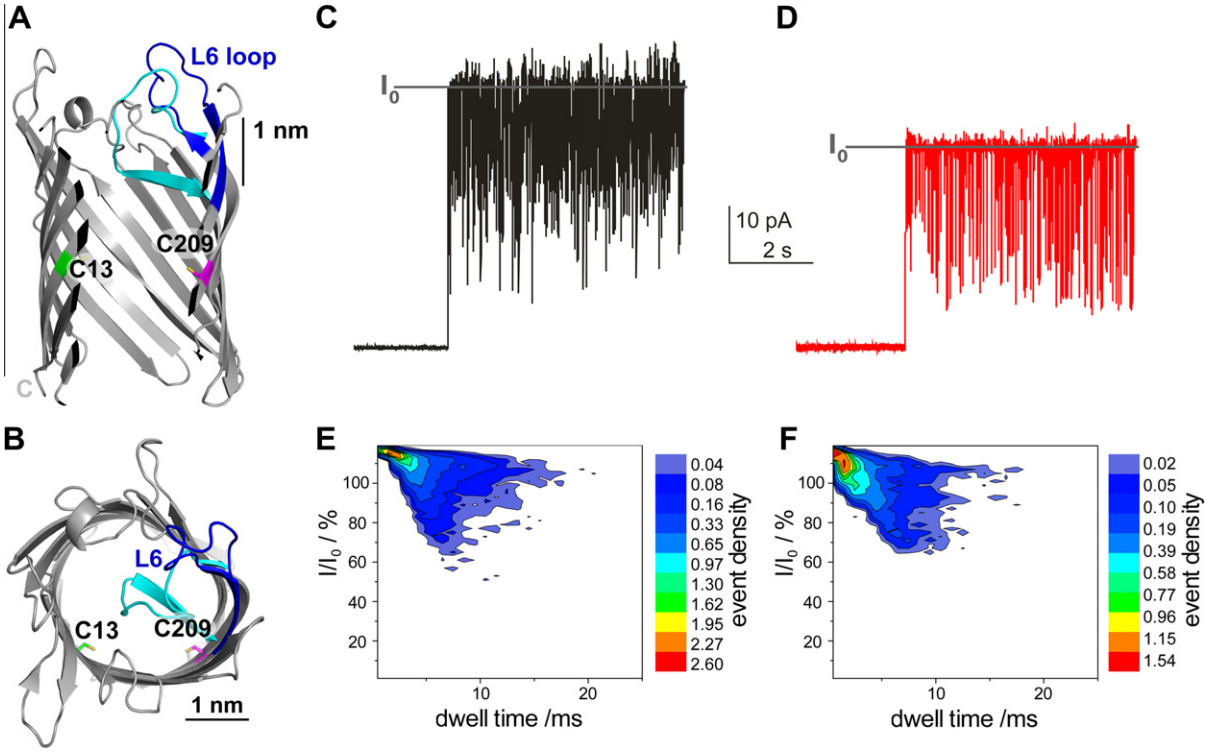

Figure 5. Analysis of flickering behavior of unmodified **OmpG/C209** and the hybrid **OmpG/C209-dansyl**. (A) open and closed state of OmpG from the side and (B) from the top. The L6 loop shown in open (blue) and closed (cyan) state. Single cysteine mutations are displayed in green (C13) and pink (C209). For the open and closed state the OmpG structures with pdb-codes: 2IWV and 2IWW were used, respectively. (C) Typical current trace of refolded **OmpG/C209**, (D) Typical trace of the **OmpG/C209-dansyl**. Both conductance traces were recorded at +60 mV, in asolectin, 1 M NaCl, 5 mM HEPES, pH 7.5. The gray lines indicate the derived conductance (I_0) used for the U/I-curve analysis. (E, F) 2D-distribution plots for dwell times versus relative current amplitudes of events in a typical current trace of **OmpG/C209** and **OmpG/C209-dansyl**, respectively. The event density is normalized to the overall number of events in the plot.

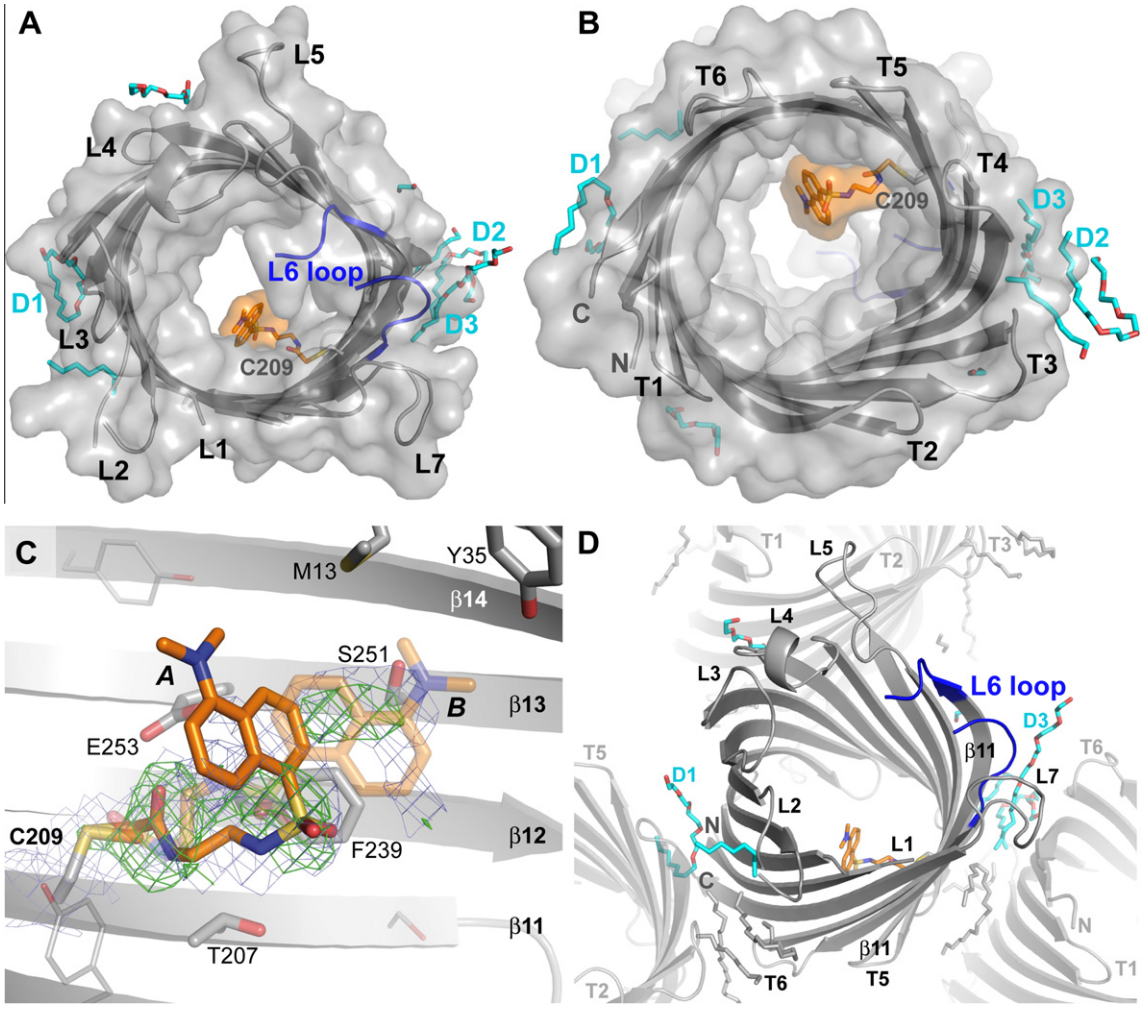

Figure 6. Crystal structure of **OmpG/C209-dansyl** with pore represented in grey, **dansyl** shown in orange and lipids shown in cyan with fully modeled lipids named D1 to D3. L6 loop is highlighted in blue. (A) Top view upon the pore with calculated surface representation (probe radius 1.4 Å). (B) View from bottom. (C) SIGMAA-weighted OMIT electron densities were calculated at 2.4 Å resolution for **OmpG/C209-dansyl** prior to model building of its **dansyl** modification. The linker region is well defined in $F_{obs} - F_{calc}$d (contouring level: 2.5 $\sigma \equiv 0.11$ e/Å^3) and $2F_{obs} - F_{calcd}$ (contouring level: 0.8 $\sigma \equiv 0.16$ e/Å^3) OMIT densities. Structural heterogeneity as shown by the **dansyl** moiety was modeled as two alternative conformations *A* and *B*, respectively. (D) View into crystal packing showing the lipids around the β-barrel as well as the symmetry-equivalent pores and lipids.

attachment of the dansyl moiety that is well defined up to the sulfonyl group. In contrast, the naphthyl moiety lacks well defined density most likely due to its mobility that is not restrained by interactions with other residues lining the wall interior. The **dansyl** unit was accordingly modeled and refined in two alternative conformations. Apart from the Y209C exchange, a comparison with the OmpG wild type structure shows no significant structural changes for residues forming the channel interior that accommodates the linker arm (T207, F239, E253) as well as the **dansyl** moiety (M13, Y35, S251, N277).

The related approach to modify the trimeric porin OmpF by incorporation of dibenzo-crown modulators showed an ordered arrangement of the synthetic modulator within the pore region only for one of the two crystal forms which became available for this porin hybrid.[10] Here, the conformation of the dibenzo-crown adopted in crystal form II was found to be sterically arrested by the L3 loop and stabilized by several interactions with the modulator's aryl group. In OmpF, the L3 loop forms the central constriction site, whereas OmpG lacks such a conformational restraint and provides a cylindrical outline for its pore lumen. The observed mobility of the **dansyl** modulator within OmpG is hence caused by a lack of steric restraints and requires in future the incorporation of additional specific modulator-protein interactions. Interestingly, the locking of synthetic modulators within the OmpF pore lasted long enough to cause a large spread of recorded specific channel conductivities. This behavior is not observed in OmpG hybrids due to apparently fast conformational changes made by the **dansyl** modulator within the pore.

3. Conclusion

The data shown underline the suitability of OmpG as a robust structural template for ion-channel engineering. OmpG hybrids can be readily produced in large amounts, characterized by black lipid membrane measurements and crystallized due to their high degree of stability. The mobility of the modulator shown might be overcome by incorporating specially adapted synthetic modulators or a more complex two-point attachment, which can be easily achieved in the OmpG pore due to its monomeric nature. The flickering characteristics of OmpG which disturb sensing could be eliminated in such designs by fixing the L6 loop as shown by Bayley and co-workers,[17] because this region is distinct from the central part of the pore most eminent for the incorporation of synthetic sensors and switches.

4. Experimental section

4.1. Expression and purification of membrane-inserted wild type OmpG

The gene encoding OmpG was amplified from genomic DNA of *E. coli* K-12 with the primers ATGGATGGCATATGAAAAAGTTATT ACCCTGTACCGCAC and GTAGGAATTCTTAATGGTGG TGGTGATGA TGGAACGAGTAATTTACGCCGACACC (restriction sites underlined) and cloned into pET20b(+) (*Novagen*).

Expression of OmpG in the outer membrane was performed in an Omp deficient *E. coli* BL21 (DE3) gold strain with the phenotype F^-, *ompT hsdS*$_B$ (r_B^- m_B^-) *gal dcm* (DE3) Δ*lamB ompF::*Tn5 Δ*ompA* Δ*ompC* Δ*ompN*.[23] Cultures were grown in LB medium containing 100 mg/L ampicillin and 1% glucose at 37 °C to an OD_{595} of 0.7 and expression was induced with 1 mM IPTG. Cells were harvested (6400*g*, 4 °C, 15 min), resuspended in lysis buffer (20 mM Tris/HCl, pH 8.0, 200 mM NaCl) and shock frozen in liquid nitrogen. Cells were broken using the Emulsiflex C5 (*Avestin*) and crude cell extract was centrifuged (25,402*g*, 30 min, 4 °C). Purification was performed according to a modified protocol from Subbarao et al.[13] The pellet was three times homogenized in TSB (20 mM, Tris/HCl, pH 8.0, 300 mM NaCl, 10% (v/v) glycerol, 1.5% (w/v) LDAO) stirred for 30 min at room temperature and centrifuged (100,000*g*, 4 °C, 1 h) respectively. The supernatants were pooled and purified via Ni-NTA affinity column (*Qiagen*) with a linear imidazole gradient from 0 to 250 mM. Further purification was performed via gel filtration (Superdex200, *GE Healthcare*) in gel filtration buffer (10 mM NaOAc, pH 5.5, 50 mM NaCl, 10% (v/v) glycerol, 0.05% (w/v) LDAO) and ion exchange chromatography (ResourceQ, *GE Healthcare*) in IEX buffer (10 mM Tris/HCl, pH 8.0, 50 mM NaCl, 10% (v/v) glycerol, 0.4% (w/v) C_8E_4) with a linear gradient to 500 mM NaCl. The product was concentrated to 10 mg/mL, dialyzed against buffer (20 mM Tris/HCl, pH 8.0, 100 mM NaCl, 10% (v/v) glycerol, 0.4% (w/v) C_8E_4) and stored at −80 °C.

4.2. Expression and purification of cysteine mutants and wild type OmpG inclusion bodies

The gene encoding OmpG without signal sequence was amplified from genomic DNA of *E. coli* K-12 strain with the primers ATGGATGGCATATGGAGGAAAGGAACGACTGGCAC and GTAGGAATTCTTA ATGGTGGTGGTGATGATGGAACGAGTAATTTACGCCGACACC (restriction sites underlined) and cloned into a pET20b(+) vector (*Novagen*).

Cysteine mutants were created via site directed mutagenesis on the basis of this **OmpG** plasmid using the primers CTTTAATATCGG CGCGTGTTACGAAATAGAAAACG for **OmpG/C13** (cysteine codon underlined) and CTCGGTGACGCCGTGTACGCGCATTG (cysteine codon underlined) for **OmpG/C209**. Expression, cell harvesting and lysis of cells was performed as described above for membrane-inserted OmpG. Subsequent purification of denatured OmpG was done according to a modified protocol from Yildiz et al.[14] The pellet containing the protein was homogenized in Triton-TEN buffer (50 mM Tris/HCl, pH 8.0, 100 mM NaCl, 10 mM EDTA, 2.5% (v/v) Triton-X-100) and repelleted (25,402*g*, 4 °C, 15 min) three times. The same procedure was repeated with TN buffer (50 mM Tris/HCl, pH 8.0, 100 mM NaCl) except for the last centrifugation step. The protein suspension was stored at −80 °C until usage.

4.3. S-Alkylation with the modulator *N*-(2-ethyl-iodo-acetamide)-dansyl

N-(2-Ethyl-iodo-acetamide)-dansyl (**dansyl**) was prepared as described before by Reitz et al.[10] and stored at −80 °C in a flask until usage.

Washed inclusion bodies of OmpG were dissolved in denaturation buffer P (100 mM Na-phosphate, pH 7.5, 6 M urea) to a final concentration of 0.1 mM. TCEP was added to a final concentration of 1 mM followed by incubation for 10 min at room temperature. Then, **dansyl** dissolved in acetonitrile was given to the mixture at a final concentration of 1 mM and the sample was incubated at 37 °C for 30 min. **Dansyl** and TCEP were added again in 10-fold excess, followed by a second incubation of 30 min and subsequent quenching of the excess reagents by 10 min incubation at room temperature with 10 mM DTT.

Prior to refolding, the reaction mixture was purified via a desalting column (PD-10, *Amersham*), that was equilibrated with denaturation buffer according to manufacturer's instructions.

The intrinsic fluorescence of **dansyl** when exited with UV light enabled the detection of OmpG–dansyl hybrids in SDS–PAGE gels.

4.4. Refolding and purification of OmpG

OmpG was solved in denaturing buffer P for modified OmpG or denaturing buffer T (25 mM Tris/HCl, pH 8.0, pH 7.5, 6 M urea) for unmodified OmpG. Protein solutions were rapidly diluted in refolding buffer P (25 mM Na-phosphate, pH 8.0) or T (25 mM Tris/HCl, pH 8.0) containing *n*-octyl-β-D-glucopyranoside (*n*-OG) at a final concentration of 3% (w/v), 1 mg/mL protein and 2.5 M urea. The mixture was stirred over night at 30 °C. Refolding was monitored via SDS–PAGE using the different apparent molecular masses of 28 kDa for the folded and 36 kDa for the unfolded state of OmpG.[11] The mixture was afterwards treated with proteinase K for 10 min at 25 °C in a concentration of 20 μg/mL, using the extraordinary stability of folded OmpG against this protease. The digestion reaction was stopped with 13 mM PMSF and the reaction mixture was kept on ice for immediate further purification.

The solution was diluted by the same volume IEX buffer and applied to a ion-exchange column (HiTrap DEAE Sepharose, *GE Healthcare*). Elution was performed with a linear gradient of 50–500 mM NaCl. The product was concentrated to 10 mg/mL, dialyzed against buffer (20 mM Tris/HCl, pH 8.0, 100 mM NaCl, 10% (v/v) glycerol, 0.4% (w/v) C_8E_4) and stored at −80 °C.

4.5. Crystallization of OmpG channels

Crystallization of OmpG and OmpG–dansyl hybrids was performed according to the published conditions by Subbarao et al.[13] using the sitting drop technique with 1 μL protein at a concentration of 5–8 mg/mL added to 1 μL of reservoir buffer (50 mM sodium cacodylate, pH 5.25–5.75, 28–32% PEG400 and 1–1.4 M sodium formate). The setup yielded crystals after about two weeks in various conditions, which could be directly flash-frozen in liquid nitrogen due to the cryo-protecting characteristics of the PEG400 precipitant.

4.6. Data collection and structure solution

Diffraction data with a resolution of 2.4 Å for the **OmpG/C209-dansyl** were collected at beam line ID14-4 at the ESRF, Grenoble, at a temperature of 100 K. Likewise, crystallographic data were recorded for native OmpG at 2.4 Å resolution at ESRF beamline ID29 to provide a reference for delineating structural changes by modification within the pore. Data were indexed and scaled using XDS and XSCALE.[24,25] Structure solution was performed using PHASER[26] (CCP4i package[27]) and the OmpG structure of Subbarao et al. (pdb code 2F1C)[13] as a search model. Refinement was performed using REFMAC5[28] (CCP4i package) giving a final R_{work}/R_{free} of 22.1/28.7 for the **OmpG/C209-dansyl** structure as shown in the refinement statistics (Table 1). Apart from some flexible loops the β-barrel was well defined and diffraction data revealed addi-

Table 1
Crystallographic table of OmpG structures

Data collection and processing	**OmpG**/wt	**OmpG/C209-dansyl**
X-ray source	ID29, ESRF	ID14-4, ESRF
Wavelength (Å)	0.8857	0.9755
Detector	ADSC Quantum Q315r	
Temperature (K)	100	
Space group	C2	
Cell dimensions		
a (Å)	98.3	99.6
b (Å)	69.5	69.8
c (Å)	58.8	59.1
β (°)	103.2	103.6
Resolution (Å)	20–2.4 (2.53–2.40)	30–2.4 (2.53–2.40)
Observed reflections	48,906	55,499
Multiplicity	3.3 (3.4)	3.6 (3.3)
Unique reflections	14,997	15,345
R_{merge}[b]	0.066 (0.318)	0.053 (0.709)
Completeness[a] (%)	98.9 (100.0)	98.9 (95.4)
$\langle I\rangle/\sigma\langle I\rangle$[a]	15.3 (5.2)	16.7 (2.2)
Mosaicity (°)	0.498	0.277
Wilson B-factor (Å^2)	46.1	59.5
Refinement statistics		
Resolution (Å)	19.8–2.40 (2.46–2.40)	30.0–2.40 (2.46–2.40)
R_{work} (%), R_{free} (%)[a,c,d]	22.0, 26.5 (31.2, 36.7)	22.1, 28.7 (26.8, 41.9)
Reflections (working set, test set)	14,231, 753	13,933, 730
Rmsd bond lengths from ideal (Å)	0.010	0.011
Rmsd bond angles from ideal (°)	1.298	1.310
Number of atoms (total; protein, hetero, water)	2242; 2104, 93, 45	2418; 2201, 143, 74
Mean *B* value (total; protein, hetero, water; Å^2)[e]	33.6 (48.4); 32.0, 68.0, 39.9	42.3 (55.4); 40.2, 72.6, 45.1

[a] Values in parentheses correspond to the highest resolution shell.
[b] $R_{merge} = \Sigma_{hkl}\,\Sigma_i\,|I_i(hkl) - \langle I(hkl)\rangle|/\Sigma_{hkl}\,\Sigma_i\,I_i(hkl)$.
[c] $R_{work} = \Sigma\,|F_{obs} - F_{calcd}|/\Sigma(F_{obs})$.
[d] R_{free} crystallographic R-factor based on 5% of the data withheld from the refinement for cross-validation.
[e] Values in parentheses correspond to mean *B* values obtained without TLS refinement.

tional electron density for the modulator with the **dansyl** moiety adopting different conformations. Restraints for the modulator were generated using a structure optimized by energy minimization using the MOE v2008.1 package (*Chemical Computing Group Inc*) and MMFF94 as force field.

Coordinates and structure factors of the **OmpG/C209-dansyl** structure were deposited in the RCSB protein data bank under accession code 2WVP.

4.7. Single-channel recordings of OmpG channels

Conductivity measurements on OmpG were performed using the BLM technique. The planar lipid membranes were prepared by painting or rising the solution surface over a 200 μm hole in a two chamber apparatus (polystyrene cuvette: CP2A, bilayer chamber: BCH-22A, *Warner Instruments*) filled equally with BLM buffer (5 mM HEPES, pH 7.5, 1 M NaCl). As membrane mixture a solution of asolectin (*Avanti Polar Lipids*, No.341601) in *n*-decane (25 mg/mL) was used. Porin (2 mg/mL) was mixed equivalently with lipid, added beside the BLM and a voltage-gradient was imposed across the membrane whilst waiting for insertion of single channels.

For current detection voltages from +120 mV to −120 mV were applied and current were detected using the Axopatch 200B patch-clamp amplifier combined with a Digidata 1200B A/D converter with pClamp 9.2 software (*Axon Instruments*). The data was collected at 5 kHz and sampled at 200 Hz for further analysis.

For each measurement a well defined baseline was taken and the difference to the stable open state was determined with the software. For each reported conductivity 15–25 separate measurements at different voltage steps were taken. Each data point of the *U*/*I*-curve was taken in account to determine the conductivity via the slope derived by linear regression.

To probe the significance of observed deviations in conductivity between recorded datasets, statistical *t*-tests were performed considering all taken data points. The deviation of the single cysteine mutants against the refolded wild type **OmpG** gave a significant deviation by a confidence level of more than 90% for **OmpG/C13** and more than 99.5% for **OmpG/C209**. In the case of the mutants bearing the modulator versus the unmodified ones the t-scores were even higher (>99.5%), stating that differences in conductivity are not on account of simple scattering of data points. In comparison, the values for specific conductivities of OmpG either prepared in vivo or in vitro by refolding is significantly below the 90% confidence level.

4.8. Fluorescence spectroscopy of OmpG/dansyl hybrids

Fluorescence measurements in solution were performed at 10 °C with a FP-6500 spectrofluorometer (Jasco) using a 10 mm light path cuvette (*Hellma*). Purified OmpG samples with a concentration of 2–3 mg/mL in buffer (20 mM Tris/HCl, pH 8.0, 100 mM NaCl, 10% (v/v) glycerol, 0.4% (w/v) C_8E_4) were excited at a wavelength of 405 nm (band widths for excitation 3 nm, emission 5 nm). The **dansyl** reference was measured in buffer comprising additionally 20% (v/v) acetonitrile. Dansyl data were normalized to a relative fluorescence of 100. OmpG spectra were scaled to represent equal sample concentrations.

Crystal fluorescence was measured with an XSPECTRA microspectrometer (*4DX Systems AB*) and a Maya2000Pro 2D FFT-CCD Spectrometer (*Ocean Optics*) using a DH-2000-BAL (*Ocean Optics*) as light source and a 405 nm FLEXPOINT Laser Diode (20 mW, 40/20FE-SMA, *Laser Components*) for excitation. Spectra were recorded at 18 °C using the SpectraSuite software package (*Ocean Optics*).[29] As samples **OmpG/C209-dansyl** crystals from the same batch that yielded crystallographic data were used to record spectra between 435 nm and 1100 nm. Afterwards the spectra were normalized to the solution spectra.

Acknowledgements

We thank the Volkswagen Stiftung for support, the European Synchrotron Radiation Facility in Grenoble and our local contacts A. Goncalves (ID14-4) and A. Popov (ID29) as well as Alan Tanovic, Claudia Schroeder and especially Petra Gnau for recording OmpG datasets and technical assistance. We thank Tobias Craan and Manuel Maestre-Reyna for discussion, Uwe Linne for mass-spectrometric analyses and Stephan Kiontke and Yann Geisselbrecht for support at the microspectrometer.

References and notes

1. Bayley, H.; Cremer, P. S. *Nature* **2001**, *413*, 226.
2. Banghart, M. R.; Volgraf, M.; Trauner, D. *Biochemistry* **2006**, *45*, 15129.
3. Bayley, H.; Jayasinghe, L. *Mol. Membr. Biol.* **2004**, *21*, 209.
4. Bayley, H. *Mol. Biosyst.* **2007**, *3*, 645.
5. Essen, L.-O.; Koert, U. *Annu. Rep. Prog. Chem., Sect. C* **2008**, *104*, 165.
6. Wu, H. C.; Bayley, H. *J. Am. Chem. Soc.* **2008**, *130*, 6813.
7. Gu, L. Q.; Braha, O.; Conlan, S.; Cheley, S.; Bayley, H. *Nature* **1999**, *398*, 686.
8. Sanchez-Quesada, J.; Saghatelian, A.; Cheley, S.; Bayley, H.; Ghadiri, M. R. *Angew. Chem., Int. Ed.* **2004**, *43*, 3063.
9. Eisenberg, B. *Proc. Natl. Acad. Sci. U.S.A.* **2008**, *105*, 6211.
10. Reitz, S.; Cebi, M.; Reiss, P.; Studnik, G.; Linne, U.; Koert, U.; Essen, L.-O. *Angew. Chem., Int. Ed.* **2009**, *48*, 4853.
11. Conlan, S.; Zhang, Y.; Cheley, S.; Bayley, H. *Biochemistry* **2000**, *39*, 11845.
12. Conlan, S.; Bayley, H. *Biochemistry* **2003**, *42*, 9453.
13. Subbarao, G. V.; van den Berg, B. *J. Mol. Biol.* **2006**, *360*, 750.
14. Yildiz, O.; Vinothkumar, K. R.; Goswami, P.; Kuhlbrandt, W. *EMBO J.* **2006**, *25*, 3702.

15. Liang, B.; Tamm, L. K. *Proc. Natl. Acad. Sci. U.S.A.* **2007**, *104*, 16140.
16. Behlau, M.; Mills, D. J.; Quader, H.; Kuhlbrandt, W.; Vonck, J. *J. Mol. Biol.* **2001**, *305*, 71.
17. Chen, M.; Khalid, S.; Sansom, M. S.; Bayley, H. *Proc. Natl. Acad. Sci. U.S.A.* **2008**, *105*, 6272.
18. Macpherson, L. J.; Dubin, A. E.; Evans, M. J.; Marr, F.; Schultz, P. G.; Cravatt, B. F.; Patapoutian, A. *Nature* **2007**, *445*, 541.
19. Bayley, H.; Cronin, B.; Heron, A.; Holden, M. A.; Hwang, W. L.; Syeda, R.; Thompson, J.; Wallace, M. *Mol. Biosyst.* **2008**, *4*, 1191.
20. Chen, M.; Li, Q. H.; Bayley, H. *Chembiochem.* **2008**, *9*, 3029.
21. Schlessinger, J.; Steinberg, I. Z.; Pecht, I. *J. Mol. Biol.* **1974**, *87*, 725.
22. Li, Y. H.; Chan, L. M.; Tyer, L.; Moody, R. T.; Himel, C. M.; Hercules, D. M. *J. Am. Chem. Soc.* **1975**, *97*, 3118.
23. Prilipov, A.; Phale, P. S.; Gelder, P.; Rosenbusch, J. P.; Koebnik, R. *FEMS Microbiol. Lett.* **1998**, *163*, 65.
24. Kabsch, W. *J. Appl. Crystallogr.* **1993**, *26*, 795.
25. Kabsch, W. *J. Appl. Crystallogr.* **1988**, *21*, 67.
26. McCoy, A. J.; Grosse-Kunstleve, R. W.; Storoni, L. C.; Read, R. J. *Acta Crystallogr., Sect. D* **2005**, *61*, 458.
27. CCP4 *Acta Crystallogr., Sect. D* **1994**, *50*, 760.
28. Murshudov, G. N.; Vagin, A. A.; Dodson, E. J. *Acta. Crystallogr., Sect. D* **1997**, *53*, 240.
29. Hadfield, A.; Hajdu, J. *J. Appl. Crystallogr.* **1993**, *26*, 839.